Elastic effects and phase segregation during the growth of thin alloy layers by molecular-beam epitaxy

François Léonard and Rashmi C. Desai
Department of Physics, University of Toronto, Toronto, Ontario, Canada M5S 1A7
(Received 12 March 1997)

We explore the effects of stress and strain on the composition modulations seen during the growth of thin solid films by molecular-beam epitaxy when phase separation is the driving mechanism for the concentration inhomogeneity. A top view of the growing thin film shows lamellar and hexagonal patterns of phase-separated domains, the elastic effects being directly responsible for the appearance of the hexagonal order. We find that in the lamellar regime, elastically deformed lamellae are separated by undeformed interfaces, while in the droplet phase, the soft component is deformed and wraps the hard component. We also discuss the effects of crystal anisotropy in our system. [S0163-1829(97)07532-2]

I. INTRODUCTION

The role of elastic effects on the morphology of thin solid films has been shown to be of prime importance. In homoepitaxy, the lattice mismatch between the substrate and the growing film can induce surface instabilities, leading to nonplanar growth fronts, while for heteroepitaxy, the difference in the lattice constants of the components can lead to a stabilization of the surface.[1] These considerations, however, neglect the fact that most of the experimental literature describes systems that are immiscible, leading to phase segregation of the components. Recently, Weatherly *et al.*[2] have studied the growth of pseudobinary semiconductor compounds under compressive and tensile strain, and found a complicated interrelation between concentration modulations and surface morphology. As is typical of thin films grown by molecular-beam epitaxy (MBE), the sign of the strain is crucial in determining the properties of the thin layer, and for some of their parameters, the flat surface is stable. Phase separation during the simultaneous deposition of different atomic species has also been studied by Adams *et al.*[3] in the highly mismatched Al-Ge system.

Recently,[4] we considered phase separation during MBE in the absence of elastic effects, and found that a lamellar pattern emerges from phase separation occurring at the surface. It was shown that the concentration modulation arises from a competition between the phase separation and the constant deposition of material on the surface. Our work, however, did not consider the important contributions originating from elastic fields. Such effects have been shown[5] to alter drastically the morphology of domains in *bulk* phase-separating systems, leading to very slow growth of the domain size with time. In particular, even for equal volume fractions of the two components, the soft phase was found to wrap around the hard phase, thereby creating hard droplets in a soft matrix.

A similar approach to the one we propose here was introduced by Ipatova *et al.*[6] and considered from an *equilibrium* perspective. As we have shown in our recent work,[4] the concentration modulations in the bulk of the thin film are *not* equilibrium morphologies, and the inherent dynamical or non-equilibrium nature of the problem is crucial in explaining the morphologies that are seen experimentally. The present paper considers the following idealized experimental situation: (i) two atomic species are deposited simultaneously on a substrate held at a temperature within the coexistence region of the binary alloy phase diagram; (ii) the diffusion proceeds along the surface only; (iii) the volume fraction of the two components are equal; (iv) surface fluctuations and surface instabilities are neglected.

Our paper is divided as follows: In Sec. II, we introduce our Ginzburg-Landau free-energy functional and dynamical equations that describe the time evolution of concentration fluctuations. In Sec. III, we present results of numerical integrations of the dynamical equations while Sec. IV gives a conclusion to our work.

II. MODEL

In this section, we start by deriving the free-energy functional for a bulk binary mixture, taking into account the elastic effects. We then obtain dynamical equations that describe the time evolution of a thin solid film grown by MBE.

A. Free-energy functional

Our derivation of the free-energy functional follows the procedure of Onuki[7] and is also presented for a more complex situation in Ref. 8. We introduce a continuous variable $\psi(\mathbf{r})$, with $\mathbf{r}$ a two-dimensional vector in the (flat) plane of the growing surface, that represents the extent of the phase segregation. The order parameter $\psi(\mathbf{r})$ is proportional to the concentration difference between the two species at local position $\mathbf{r}$. A second variable $\mathbf{u}(\mathbf{r})$, the displacement vector, represents the displacement from the local equilibrium position due to elastic deformations. For single-component cubic crystals in d dimensions,[9] the elastic free-energy functional can be written as

$$\mathcal{F}_{\mathrm{el}}[\mathbf{u}] = \int d\mathbf{r}\left[\frac{1}{2}K(\nabla\cdot\mathbf{u})^2 + M\sum_{i,j}\left(\mu_{ij} - \frac{\delta_{ij}}{d}\nabla\cdot\mathbf{u}\right)^2 + \frac{1}{2}B\sum_i \mu_{ii}^2 + \alpha\psi\nabla\cdot\mathbf{u}\right], \quad (1)$$

with the last term added to describe the change of local lattice constant a with composition. The strain tensor $\mu_{ij} = (\nabla_j u_i + \nabla_i u_j)/2$. The constants K, M, and B are related to the elastic moduli in the Voigt notation as $M = C_{44}$, $K = C_{12} + (2/d)C_{44}$ and $B = C_{11} - C_{12} - 2C_{44}$. The degree of anisotropy of the crystal is represented by the parameter $\xi = B/M$, which is considered a small quantity in the present work.

In the case of binary systems, the free-energy functional has to be augmented to describe the miscible and immiscible regions of the phase diagram. For this purpose, the essential characteristics of the system can be obtained from the Ginzburg-Landau free-energy functional,

$$\mathcal{F}_{\rm GL}[\psi,\mathbf{u}] = \int d\mathbf{r}\left[\frac{-r}{2}\psi^2 + \frac{u}{4}\psi^4 + \frac{c}{2}(\nabla\psi)^2\right], \qquad (2)$$

where r is proportional to the temperature difference $T_c - T$, with T_c the critical point *without* elastic fields. The total free-energy functional $\mathcal{F}[\psi,\mathbf{u}]$ is just the sum of $\mathcal{F}_{\rm GL}$ and $\mathcal{F}_{\rm el}$. To make a connection with real systems, we note that in the homogeneous phase ($\psi = constant$), the stress is $\sigma_{ij} = \alpha\psi\delta_{ij}$, implying that the constant α can be obtained from $\ln a = -(\alpha\psi/dK)$. Thus, slow local variations in ψ and K can lead to slow local variations in the lattice constant a.

To take into account the change in the elastic moduli with composition, we expand the moduli to first order in the concentration variable ψ:

$$M = M_0 + M_1\psi,$$

$$K = K_0 + K_1\psi, \qquad (3)$$

$$B = B_1,$$

and assume that the coefficients M_1, K_1, and B_1 are small, implying $\xi = B_1/M_0$. Because the time scale to reach positional order is much smaller than the diffusion time, we make the assumption that mechanical equilibrium is instantaneously achieved, in order to adjust to a given spatial distribution of ψ. This provides a way to obtain the displacement variable $\mathbf{u}$ as a function of ψ, leading to effective long-range contributions to the free-energy functional. As shown in the Appendix, substitution of the resulting expression for $\mathbf{u}$ in $\mathcal{F}_{\rm el}$ yields an effective free-energy functional that is a function of ψ only:

$$\mathcal{F}_{\rm el}[\psi] = \int d\mathbf{r}\left[-\frac{\alpha^2}{2C}\psi^2 + \frac{\alpha^2\xi M_0}{2C_0^2}\psi^2 + f_E + f_\xi\right], \qquad (4)$$

with the free-energy densities f_E and f_ξ given by

$$f_E = \frac{M_1\alpha^2}{C_0^2}\psi\sum_{i,j}\left(\nabla_i\nabla_j W - \frac{\delta_{ij}}{d}\psi\right)^2 \qquad (5)$$

and

$$f_\xi = -\frac{\alpha^2\xi M_0}{2C_0^2}\sum_{i\neq j}(\nabla_i\nabla_j W)^2, \qquad (6)$$

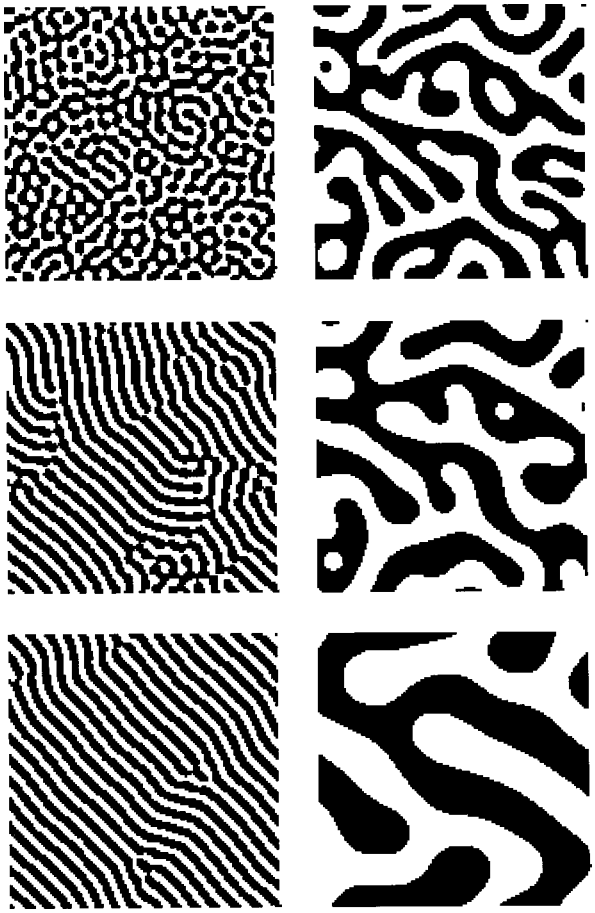

FIG. 1. The left column shows the concentration field in the near onset regime when $g_E = g_\xi = 0$ and $v = 0.24$. The right column is for $g_E = g_\xi = 0$ and $v = 0.001$ (far from onset). Times from top to bottom are $\tau = 100, 1500$, and 10 000. Black, $\phi > 0$; white, $\phi < 0$. In this and other figures, systems are of size 128×128.

and the constant $C = K + 2M_0 - 2M_0/d$ (this definition for C absorbs the contribution coming from K_1). Also, W is related to ψ through the solution of Eq. (A8), and gives the *nonlocal* nature to the free-energy functional. We now discuss the different contributions to the free-energy functional. The contributions proportional to ψ^2 in Eq. (4) simply renormalize the ψ^2 coefficient in $\mathcal{F}_{\rm GL}$, which changes the critical temperature by a constant factor (the critical point occurs when the coefficient of ψ^2 is zero). Hence, we redefine r as $r \to r + (\alpha^2/2C) - (\alpha^2\xi M_0/2C_0^2)$. The contribution f_E corresponds to a long-ranged interaction leading to shape deformations of precipitates in a matrix.[5] f_E is proportional to M_1, which means that the difference in the shear moduli between the two components is essential to obtain this contribution. The cubic anisotropy term f_ξ leads to spinodal decomposition along the soft directions [01] and [10], creating elongated domains[10] in the absence of external stresses.

The free-energy functional may be rescaled to dimensionless form using the transformations $\mathbf{x} = (r/c)^{1/2}\mathbf{r}$ and $\phi(\mathbf{x},t) = (u/r)^{1/2}\psi(\mathbf{r},t)$. With this, we obtain

$$\mathcal{F}[\phi] = \int d\mathbf{x}\left[-\frac{\phi^2}{2} + \frac{\phi^4}{4} + \frac{(\nabla\phi)^2}{2} + g_E\phi Q_E + g_\xi Q_\xi\right], \qquad (7)$$

with $g_E=(M_1\alpha^2)/(C_0^2\sqrt{ru})$, $g_\xi=-(\alpha^2 M_0\xi/2C_0^2u)$ and the functions Q_E and Q_ξ defined as

$$Q_E=\sum_{i,j}\left[\nabla_i\nabla_j W-\frac{\delta_{ij}}{d}\phi\right]^2 \tag{8}$$

and

$$Q_\xi=\sum_{i\neq j}(\nabla_i\nabla_j W)^2. \tag{9}$$

The rescaled function W satisfies $\nabla_{\mathbf{x}}^2 W=\phi$. Note that the elastic term destroys the symmetry between the two phases, implying that the equilibrium value of ϕ is no longer ± 1.

B. Dynamical equations

The time evolution of the alloy thin film is initiated by the simultaneous deposition of the two components on a flat substrate. The interactions with the substrate are neglected, as well as fluctuations in the free surface. Because the surface diffusion coefficient is much larger than the bulk diffusion coefficient, we assume that all of the atomic motions occur at the free surface. Also, the coupling between the surface layer and the bulk is neglected. Hence, the system is modelled as a two-dimensional flat square, with periodic boundary conditions, representing the top view of a three-dimensional thin film. Because the bulk diffusion is not included, a vertical cross section of the thin film can be obtained through the history of the surface layer.

The diffusion[4] in the surface plane is governed by inhomogeneities in the chemical potential and by the requirement that the average concentration must be fixed. The constant deposition of material on the surface tends to draw the value of $\phi(\mathbf{x})$ towards the average concentration in the incoming beam (we take this average to be zero in the following, which is equivalent to the deposition of a symmetric 50-50 mixture). The time evolution of ψ is

$$\frac{\partial\psi}{\partial t}=\Lambda\nabla^2\frac{\delta\mathcal{F}}{\delta\psi}-\Gamma\psi, \tag{10}$$

where Λ is a kinetic coefficient and Γ is proportional to the deposition rate. With the time rescaling $\tau=(\Lambda r^2/c)t$, the time evolution of the dimensionless variable ϕ is

$$\begin{aligned}\frac{\partial\phi}{\partial\tau}&=\nabla^2(-\phi+\phi^3-\nabla^2\phi+g_E Q_E)\\&\quad+2g_E\sum_{i,j}\nabla_i\nabla_j\phi[\nabla_i\nabla_j W-\tfrac{1}{2}\delta_{ij}\phi]\\&\quad+g_\xi\sum_{i\neq j}\nabla_i^2\nabla_j^2 W-v\phi,\end{aligned} \tag{11}$$

with $v=(c\Gamma)/(\Lambda r^2)$. We will refer to the important parameter v as the deposition rate. Note that a linear term like $-v\phi$ also occurs in the relaxational dynamics models for microphase separation kinetics in block copolymers.[11] In this equation, we have neglected fluctuations in the order parameter coming from thermal and beam noise, which we incorporate as initial conditions on ϕ. In the absence of a deposition process ($v=0$), various cases have been studied. For $g_E=g_\xi=0$, a quench from an initial homogeneous state to a point in the coexistence region of the phase diagram leads to spinodal decomposition and formation of domains that grow in time as $\tau^{1/3}$.[12] When only the anisotropic contribution is present ($g_E=0$, $g_\xi\neq 0$), the dispersion relation has a maximum value along the [01] or [10] directions, leading to needlelike domains[13] with the longer direction oriented in [01] or [10]. In the presence of the elastic interaction only ($g_E\neq 0$, $g_\xi=0$),[5] the elastic energy slows the domain growth, with a saturation of the average domain size at late

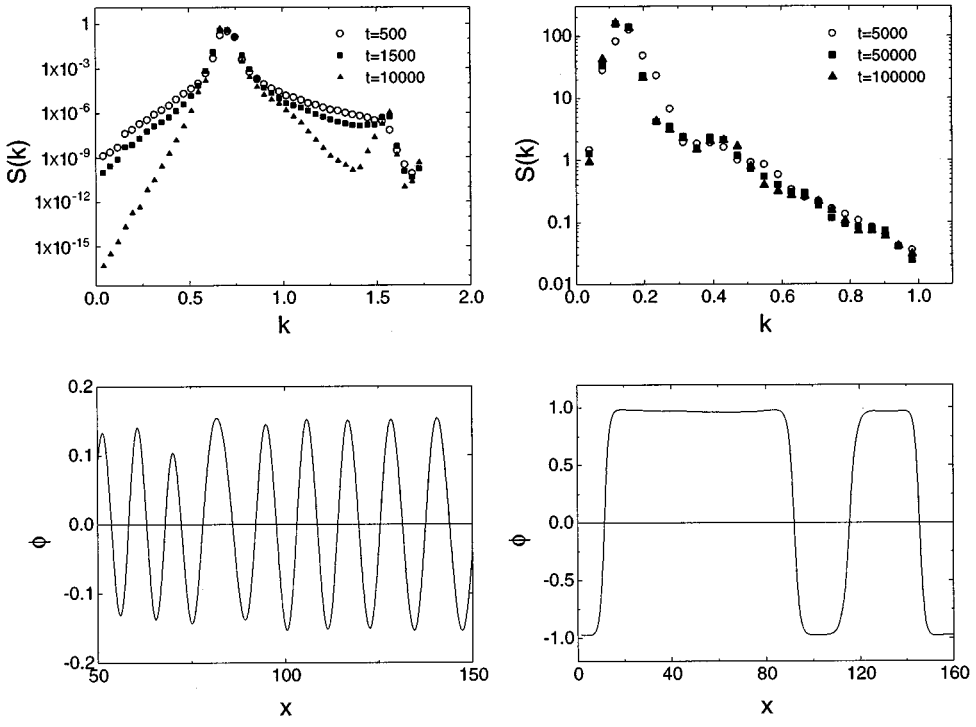

FIG. 2. The left (right) column shows the structure factor and the order parameter along a horizontal cut at $\tau=10\,000$ for the near-onset (far-from-onset) regime. The times for the structure factor correspond to those in Fig. 1.

FIG. 3. A vertical cross section of the thin film taken along the x direction. The bottom configuration shows the appearance of the thin film at early times ($0<\tau<100$), while the top configuration corresponds to the steady state ($1400<\tau<1500$). The lateral size of the system is 128 and the vertical scale is chosen to show details.

times. The system consists of ellipsoidal hard domains in a soft percolated matrix (the saturated hard domain size scales as $1/g_E$). Finally, the presence of both the elastic term and the anisotropy creates saturated hard cuboidal domains in the soft matrix.[14] In the case of alloy growth by MBE without elastic effects ($g_E=0$, $g_\xi=0$), the deposition rate v is a crucial parameter in determining the stability of the alloy to

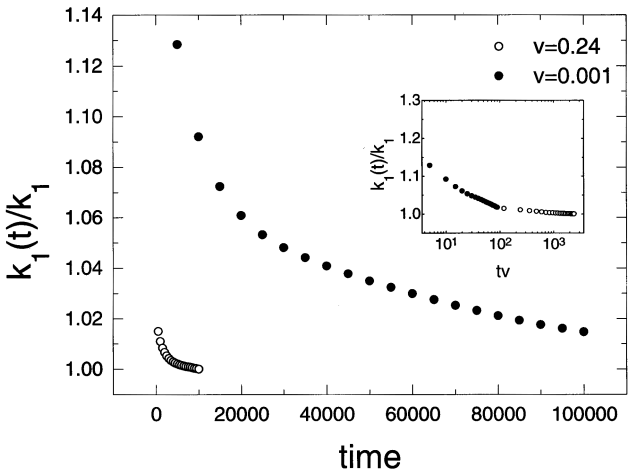

FIG. 4. The wave number as a function of time in the near-onset (open circles) and the far-from-onset regimes (solid circles), corresponding to Fig. 1. The scaled function $g(tv)$ is shown in the inset.

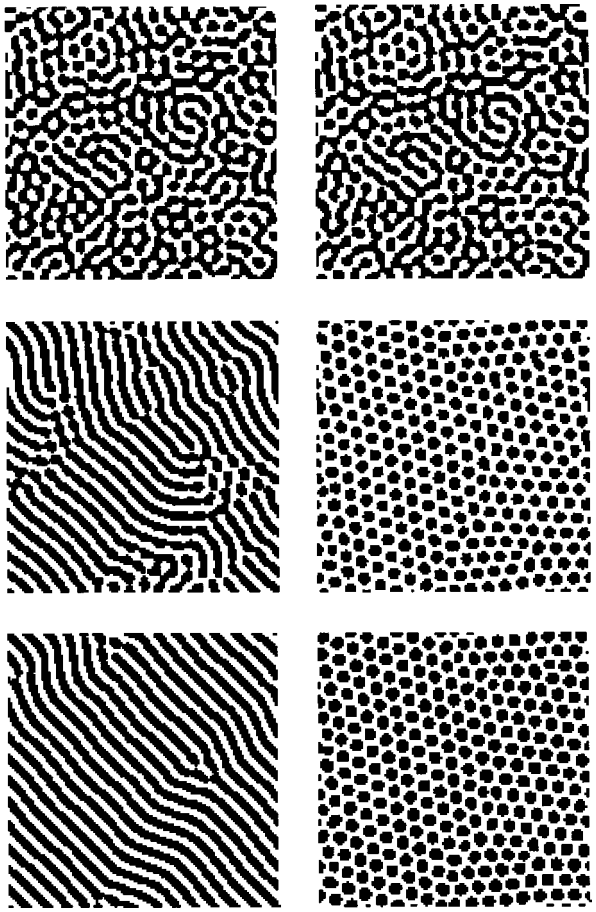

FIG. 5. The left column shows the concentration field in the near-onset regime when $g_E=0.05$ and $v=0.24$. The right column is for $g_E=0.5$ and $v=0.24$. Times from top to bottom are $\tau=100$, 1500, and 10 000. $g_\xi=0$ in this figure.

phase segregation: note that Eq. (11) simplifies to $\partial\phi/\partial\tau=\nabla^2(-\phi+\phi^3-\nabla^2\phi)-v\phi$, which has been studied previously in connection with microphase separation in block copolymers[11] and the laser-induced melting phenomena in the limit of the large latent heat of the substrate.[15] From these studies we infer that for ($g_E=0$, $g_\xi=0$), $v=1/4$ is a critical value of the deposition rate. If the deposition rate $v<1/4$, lamellar patterns appear with a v-dependent modulation wavelength; if $v>1/4$, the constant burial of surface domains by the incoming beam suppresses the phase separation, and the thin film is homogeneously mixed.[4] The present work concentrates on the case where $v<1/4$ and studies the elastic and anisotropic effects on the time evolution and the steady state of the system.

III. RESULTS

The Langevin equation [Eq. (11)] was discretized in space and time using a finite-difference scheme, and integrated using the Euler method. The results reported here correspond to simulations on a 128×128 square grid with periodic boundary conditions. We believe that finite-size effects were minimal since the selected wavelength of the modulation in the steady state is much smaller than the system size. The mesh size and time step were chosen as $\Delta x=1.25$ and $\Delta t=0.1$. A discrete, isotropic form for the Laplacian was

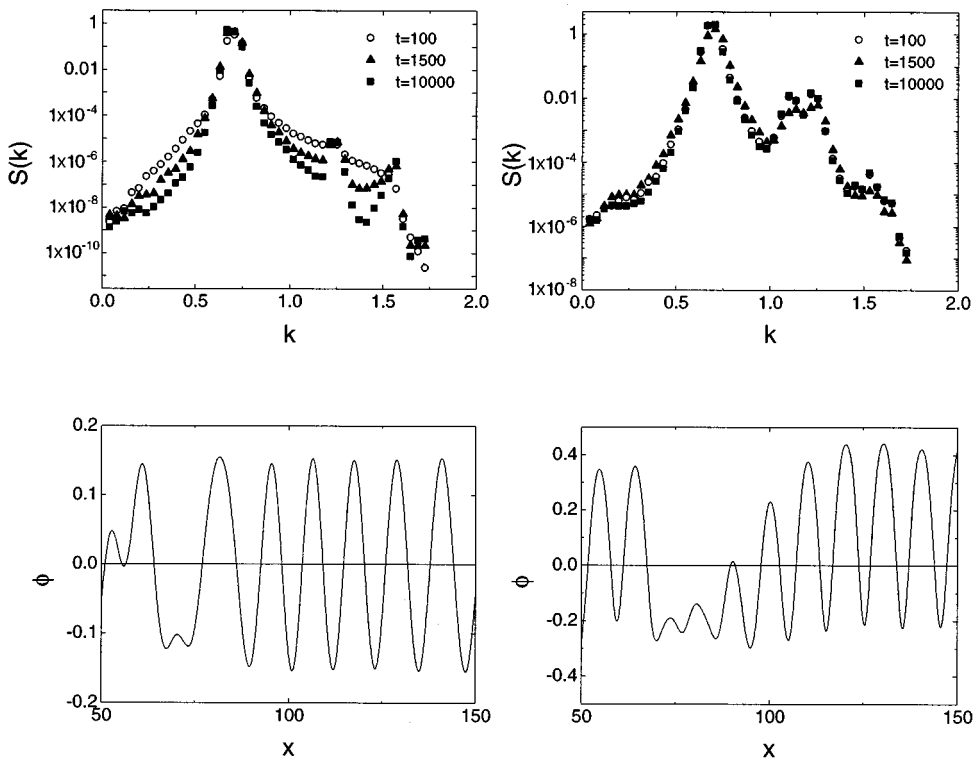

FIG. 6. The structure factor and the order parameter along a horizontal cut at $\tau = 10\,000$ in the near-onset regime. Left column: $g_E = 0.05$. Right column: $g_E = 0.5$. The times for the structure factor correspond to those in Fig. 5.

used,[15] while the field W was obtained using Fourier transform methods. The initial state of the system consists of a random distribution of ϕ in the range $(-0.1,0.1)$. Due to the length and size of the simulations, averages were taken over one to four runs with different initial conditions. For the deposition rate $v > 1/4$, the initial homogeneous state is stable. The onset of thermodynamic instability for $v < 1/4$ leads to phase segregation. Hence, in what follows, we take $v < 1/4$ and study the effects of g_E and g_ξ. We start with results for $g_E = g_\xi = 0$, establishing basic results and a basis for comparison.

A. $g_E = 0$, $g_\xi = 0$, and $v \neq 0$

This case corresponds to MBE growth at deposition rate v with no elastic or anisotropic effects. Figure 1 shows configurations for the field ϕ at different times. On the left, the parameter $v = 0.24$, close to the onset of instability at $v = 1/4$, and the wavelength of the pattern is close to the maximally unstable wavelength, $\lambda = 2\sqrt{2}\pi$. This regime will be referred to as the near-onset regime. The right column is for $v = 0.001$ (far from onset regime). There, the wavelength of the modulation is much larger than in the near-onset regime, and the value of the order parameter changes from $+1$ to -1. The differences between the two regimes is also shown in Fig. 2, where the circularly averaged structure factor,

$$S(k) = \langle |\phi(k)|^2 \rangle, \tag{12}$$

and the profile of the order parameter along a horizontal cross section are plotted. Initially, the order parameter grows exponentially in time, with segregation in two phases. The initial maximally unstable wave number is $k \approx 1/\sqrt{2}$, which then decreases to attain its steady-state value. At the same time, stripes form and orient themselves locally. Once k is saturated, the ordering proceeds through the elimination of defects. In the near-onset regime, the wavelength of the modulation can be calculated[4] to be $\lambda \sim v^{-1/4}$, while far from onset, $\lambda \sim v^{-1/3}$. Furthermore, the appearance of the lamellar patterns can be explained by appropriately constructing an effective free-energy functional such that $\partial\phi/\partial\tau = \nabla^2(\delta F_{\rm eff}/\delta\phi)$. The effective free-energy functional contribution due to v is repulsively long range, which competes with the attractive short-range interaction. Near onset, the amplitude of the modulations (proportional to the concentration difference in a real alloy) is small and scales as

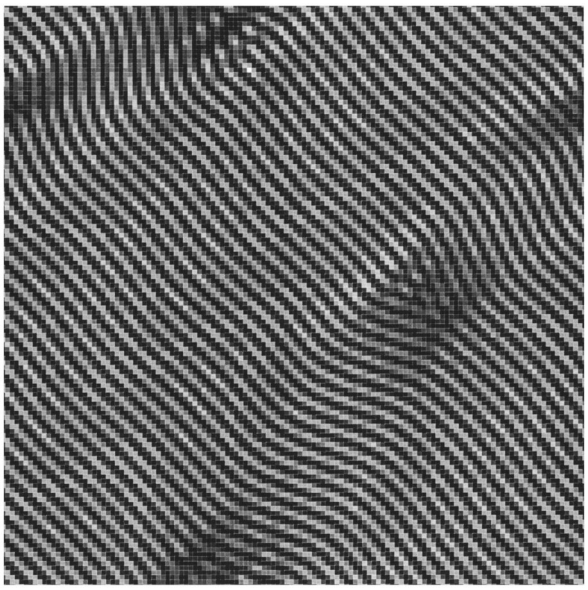

FIG. 7. Gray-scale plot of the degree of deformation Q_E for the last lamellar configuration of Fig. 5. Black represents $Q_E = 0$, while white represents $Q_E = 0.014$.

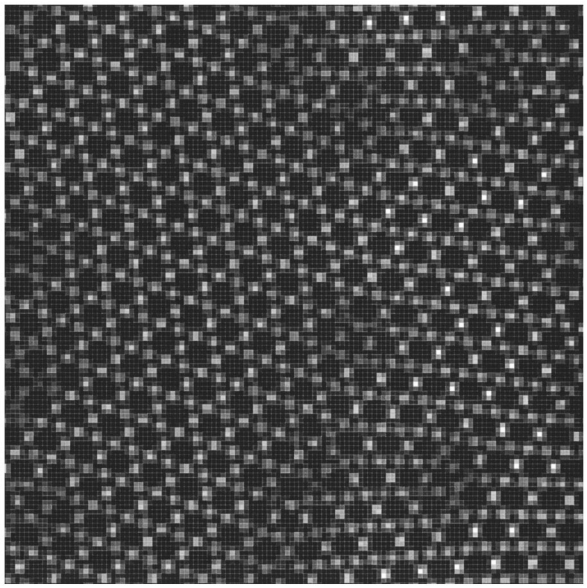

FIG. 8. Gray-scale plot of the degree of deformation Q_E for the last hexagonal configuration of Fig. 5. Black represents $Q_E=0$, while white represents $Q_E=0.1$.

$\sqrt{1/4-v}$; the single-mode approximation is excellent very close to onset. For small values of v, the order parameter is equal to ± 1 within the bulk of the domains, which are separated by thin interfacial regions; the number of modes needed to describe the profile increases as v decreases.

A vertical cross section of the thin film can be considered if one makes a correspondence between the time scale for diffusion and the velocity at which the free surface is growing. Figure 3 shows a cross section corresponding to a horizontal cut in Fig. 1 (the correspondence between the surface height and time has been chosen to show details). Note that the appearance of the cross-sectional configurations depends on the direction chosen, which is in agreement with transmission-electron-microscopy experiments.[16] After deposition of a few monolayers (bottom configuration) clear vertical structures appear in the thin film. At late times, the wavelength of the modulation is saturated, and the top layers of the alloy film consists of vertical columns of alternating concentration. To better characterize the appearance of the cross section, we calculated the average wave number as a function of time (or film thickness) from the first moment of the structure factor

$$k_1=\frac{\int_0^\infty kS(k)dk}{\int_0^\infty S(k)dk}. \tag{13}$$

Figure 4 shows k_1 as a function of time for the near-onset and the far-from-onset regimes. Near onset, k_1 saturates rapidly to a value ≈ 0.7, while for small v, the wave number decreases over a wide time scale. In fact, Yeung and Desai[15] have shown that not too close to onset, the wave number satisfies the scaling form $k(t,v)=k_\infty(v)g(tv)$, with $k_\infty(v)$ the steady-state wave number. The function $g(x)\sim x^{-1/3}$ for small x, and $g(x)\sim$ *constant* for large x. The insert in Fig. 4 shows the scaled function $g(tv)$. It also shows that the data shown in this figure correspond to the crossover regime of the function $g(x)$.

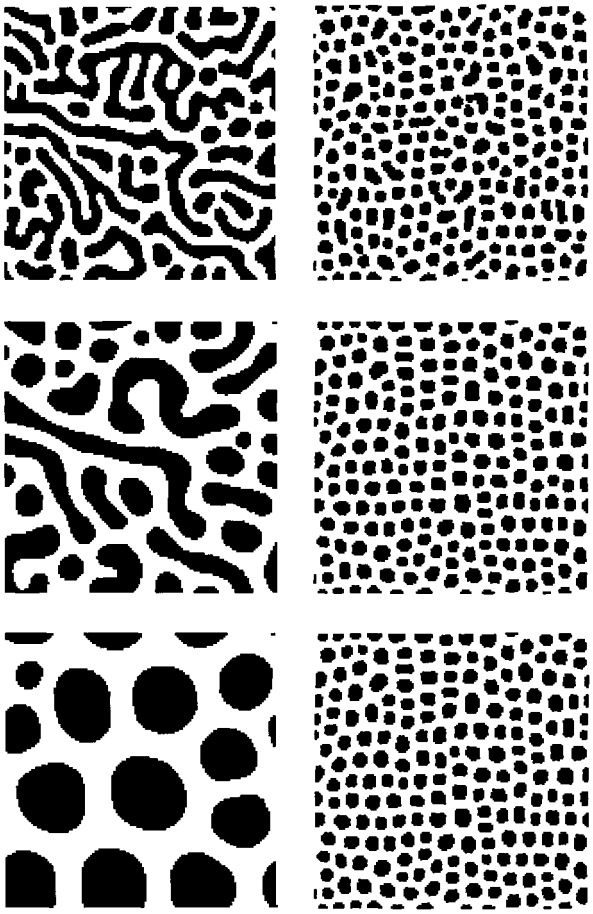

FIG. 9. The left column shows the concentration field in the far-from-onset regime when $g_E=0.05$ and $v=0.001$. The right column is for $g_E=0.5$ and $v=0.1$. Times from top to bottom are $\tau=100$, 1500, and 100 000. $g_\xi=0$ in this figure.

B. $g_E\neq 0$, $g_\xi=0$, and $v\neq 0$

When $g_E\neq 0$, we expect that the competition between the long-range interaction and the saturation of the domain size due to the elastic effects will lead to new ordered structures. Figure 5 shows the time evolution of the concentration field near the onset of instability ($v=0.24$) for $g_E=0.05$ (left column) and $g_E=0.5$ (right column). In these figures, the locations of the grid points were corrected for the displacement **u**. For the smallest value of g_E, the system orders in a lamellar phase very similar to the case $g_E=0$. Differences between Fig. 1 and Fig. 5 can be seen where crystalline defects are present. For $g_E=0.5$, droplets of the hard phase form in a soft matrix and order themselves to create an hexagonal pattern (the distribution of droplet sizes is sharp). The appearance of the hexagonal phase here is special because for $g_E=0$, the lamellar phase is always seen if the volume fraction of the two components is the same. Because of conservation of material, there is a relation between the value of the order parameter in the phases and the area occupied by the droplets. For the hexagonal and the lamellar order, the fraction of the area occupied by the hard droplets is $-\phi_s/\Delta\phi$, with ϕ_s the order parameter in the soft phase and $\Delta\phi=\phi_h-\phi_s$. Further characterization of the film surface can be found in Fig. 6, where the structure factor and the order parameter are plotted. The order parameter profile

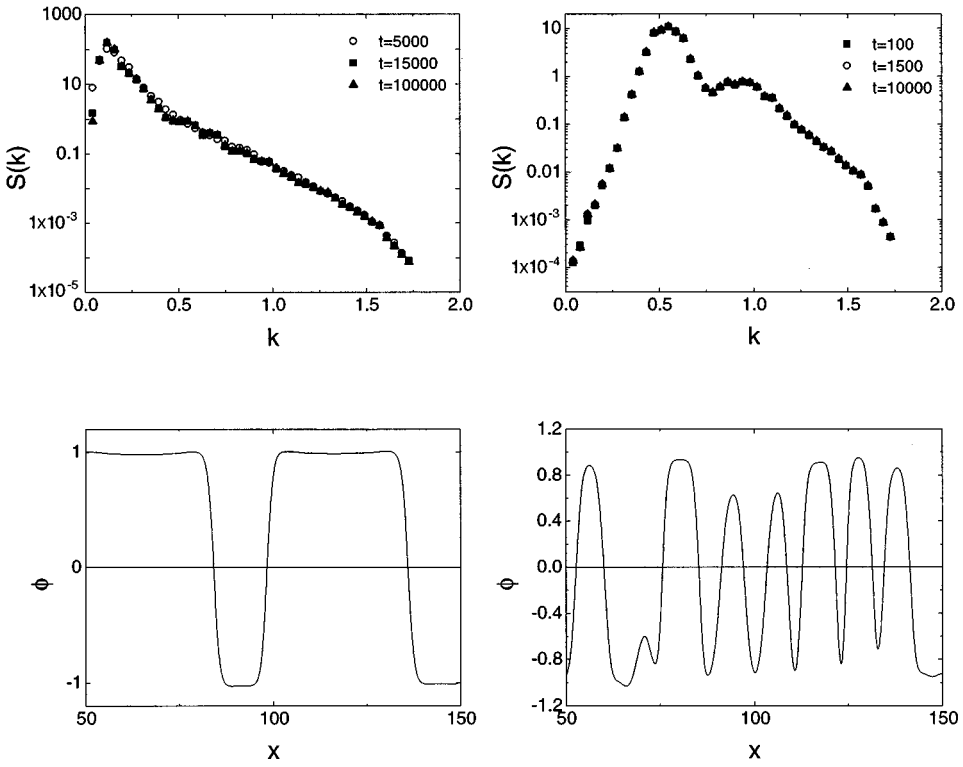

FIG. 10. The left column shows the structure factor and the order parameter along a horizontal cut at $\tau = 10\,0000$ for the left column, and at $\tau = 10\,000$ for the right column, in the far-from-onset regime. Left column: $g_E = 0.05$. Right column: $g_E = 0.5$. The times for the structure factor correspond to those in Fig. 9.

shows clearly the difference in the saturation value of the concentration field in the hard and the soft phases. Peaks in the scattering intensities describe the crystalline ordering, with the position of the first peak at $k = 2\pi/\lambda$ for the lamellar phase (λ is the wavelength of the order parameter modulation) and at $k = 4\pi/(\sqrt{3}D)$ for the hexagonal phase (D is the distance between the center of neighboring droplets).

To describe the elastic deformation of the system, we computed the function Q_E. The gray-scale contour plot of Fig. 7 corresponds to the last configuration for the lamellar phase in Fig. 5. Both the hard phase ($\phi > 0$) and the soft phase ($\phi < 0$) show elastic deformations, while the interfaces between the two phases are not deformed. In this regime $\Delta\phi$ is small and the elastic interactions do not alter drastically the final configurations. In fact, if we assume that the order parameter is given by $\phi(x) = \phi_0 \cos(kx)$, then $Q_E = \frac{1}{2}\phi_0^2 \cos^2(kx)$, which is in excellent agreement with Fig. 7. For larger values of g_E, the function Q_E (Fig. 8) shows that the soft phase wraps the hard phase in such a way as to minimize the deformation of the hard phase, thereby creating droplets. The long-range effect of the deposition rate then orders the droplets in the hexagonal array. Q_E takes its maximum value in the thinner regions of the soft phase, which appear six times around a droplet. We note that transmission-electron-microscopy measurements are sensitive to fluctuations of the local lattice parameter.[17] Hence, our pictures can give a correspondence with such measurements.

Far from the onset of instability (i.e., for a slow deposition process), $\Delta\phi$ is at its maximum, and domains of the two phases are separated by sharp interfaces. Because f_E is proportional to $\Delta\phi$, it becomes more important in this regime. As Fig. 9 illustrates, the final state of the deposition process consists of deformed droplets, even for $g_E = 0.05$. For this smaller g_E value, the time evolution of the system proceeds through the formation of an interconnected network which then breaks up. Long stripes become unstable and pinch away to form droplets. In Fig. 10, we show the structure factor and the order parameter profile.

For $g_E = 0.5$, droplets form quickly, due to the larger elastic energy. The far from onset steady state consists of deformed droplets with flattened interfaces between neighbor droplets. Also, the size distribution is not as sharply peaked as compared to the near-onset results. Figure 10 shows that the structure factor possesses a strong peak around $k = 0.55$ and a secondary peak at $k = 1$, still representative of the underlying hexagonal structure. However, the two peaks are broadened by the distortions in the lattice order and the size of the droplets. The flattening of the sides of droplets is due to shape changes of the hard domains from spheres to plates in order to minimize the elastic energy. This is shown in Fig.

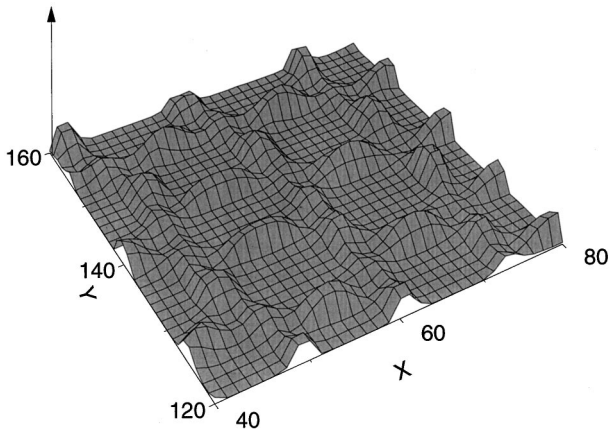

FIG. 11. The elastic deformation, Q_E, for a portion of the last droplet configuration in Fig. 9.

11, where it can be seen that Q_E is zero inside of the hard domains, while the soft phase has its maximum elastic energy in the thin regions separating the hard domains. Such shape adjustments of the hard domains have been studied by Onuki and Nishimori[18] where they showed that for bulk phase separation in the presence of elastic misfits, hard precipitates are deformed in order to cancel the elastic field produced by nearby precipitates.

It is very instructive to consider the time evolution towards the droplet phase by looking at the function Q_E. As can be seen in Fig. 12, the initial elastic deformation is similar to the near-onset regime: deformed stripes separated by undeformed interfaces. As time proceeds, the value of the order parameter difference increases and the elastic contribution becomes more important. The contribution to the energy coming from deformations inside of hard domains become too costly, leading to a bending of straight interfaces to produce droplets. The instability of straight interfaces (and of the lamellar phase) can be understood as follows:[13] in the far-from-onset regime, we suppose that we have a straight interface separating two uniaxially deformed regions. The interface is located at $x=0$, and the order parameter goes to $\phi_{\pm}$ far from the interface. We allow for fluctuations in the order parameter around the interface profile $\phi=\phi_0(x)+\phi_0'(x)\Sigma_k\delta_k(t)e^{iky}$ and calculate the change in the free energy to $O(\delta_k^2)$. We find that

$$\delta F_{\rm el}\propto\sum_k\left[\sigma k^2+\frac{1}{2}g_E(\Delta\phi)^2\lambda k-\frac{\gamma v}{k}\right]|\delta_k|^2, \qquad (14)$$

where λ is the average of the strain in the two phases and σ and γ are constants that depend on the form of $\phi_0(x)$. The time dependence of δ_k is given by the equation

$$\frac{\partial\delta_k}{\partial t}=-Dk^2\left[\sigma k+\frac{1}{2}g_E(\Delta\phi)^2\lambda+\frac{\gamma v}{k^2}\right]\delta_k, \qquad (15)$$

implying that the interface is unstable when $\sigma k+1/2g_E(\Delta\phi)^2\lambda+\gamma v/k^2<0$. This last result means that the lamellar phase becomes unstable when

$$v<\left(\frac{g_E(\Delta\phi)^2\lambda}{4\gamma^{1/3}\sigma^{2/3}}\right)^3, \qquad (16)$$

i.e., the threshold value for $v\sim g_E^3$. For values of v close to onset, the above analysis is no longer valid, and a single mode approximation shows that the critical line has negative second derivative, and eventually meets with the far-from-onset line. To appropriately calculate the ''nonequilibrium steady-state phase diagram,'' consideration of more than one mode is essential, as well as the possibility of phase coexistence. Such calculations have not been carried out.

The wavelength of the concentration modulation in the steady state as a function of the deposition rate is plotted in Fig. 13. In the absence of elastic interactions, $k_{\rm ss}\sim v^{1/4}$ near $v=1/4$, while $k_{\rm ss}\sim v^{1/3}$ for small v. When elastic interactions are present, the near-onset relation still holds, but the far-from-onset behavior is different. For small v, the elastic effects are responsible for the appearance of droplets, which

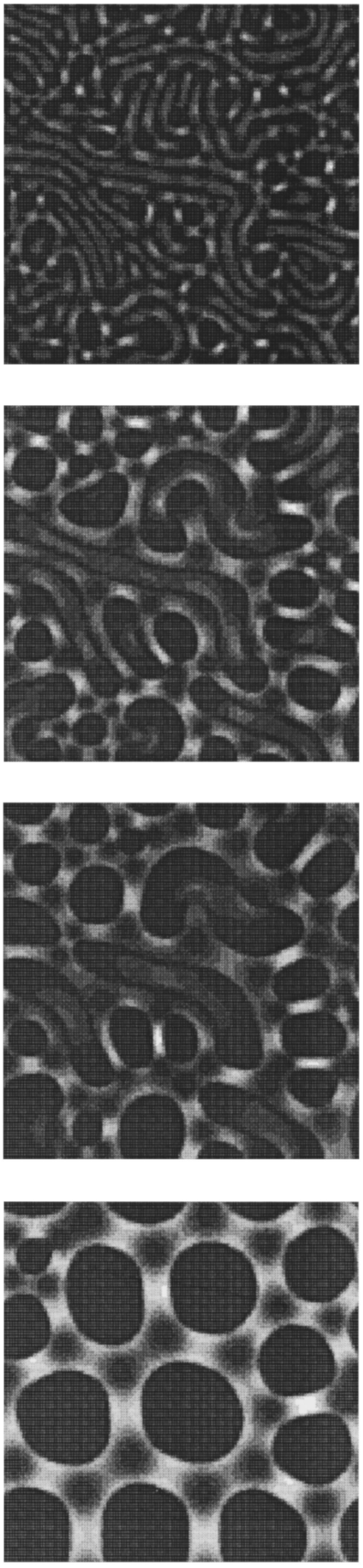

FIG. 12. Time evolution of Q_E in the far-from-onset regime for $g_E=0.05$. The straight lamellar interfaces become unstable and bend to form droplets. Panels from top to bottom correspond to time=100, 500, 1500, and 100 000.

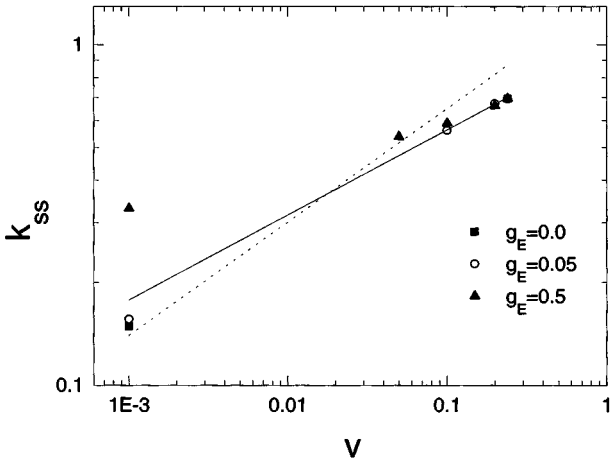

FIG. 13. Steady-state wave number as a function of the deposition rate. The lines are the near onset expansion (solid) and the far-from-onset expansion (dashed) for $g_E=0.0$.

decreases the wavelength and increases the wave number. Thus, at fixed deposition rate, the wave number increases with g_E.

C. $g_E \neq 0$, $g_\xi \neq 0$, and $v \neq 0$

In this section, we discuss how the cubic anisotropy, which is present in many III-V alloys, alters the findings of the previous sections. Figure 14 shows order parameter and Q_E configurations for $v=0.24$, $g_E=0.05$ and $g_\xi=0.1$ (see Figs. 1 and 5 for comparison). The phase segregation occurs preferentially along the [01] and [10] directions, leading eventually to a perfectly ordered lamellar structure (not shown in the figure). Interestingly, the stripes have bubbles and necks, which are mostly found at the boundaries between different stripe orientations for the latest time shown. These bubbles are due to the elastic energy, as can be seen in the gray-scale plots of Q_E. Within the ordered lamellar regions, the deformation is inside of the stripes, which are separated by undeformed interfaces. The competition between stripe orientations at boundaries creates *deformed* elastic droplets, thereby creating the bulges seen in the concentration field. Far from the onset of instability (Fig. 15) the droplets are now cuboids with their flat sides oriented along [01] or [10] (compare with Fig. 9).

IV. DISCUSSION

Our results show a number of interesting competing effects during the growth of the heteroepitaxial film. First, there is a competition between the phase separation and the constant deposition of material on the surface, leading to the formation of lamellar structures in the absence of elasticity. These lamellar structures appear below a certain threshold deposition rate, while above this threshold the film is homogeneously mixed. The deposition of material can be viewed as a *nonlocal repulsive* interaction of the form $-v\int d\mathbf{r}d\mathbf{r}'\phi(\mathbf{r})G(\mathbf{r},\mathbf{r}')\phi(\mathbf{r}')$ with $\nabla^2 G(\mathbf{r},\mathbf{r}')=\delta(\mathbf{r}-\mathbf{r}')$. Because this contribution is quadratic in ϕ, it changes the linear dispersion relation. When elastic fields are introduced with first-order dependence of the elastic moduli on concentration, there appears another long-range interaction due to

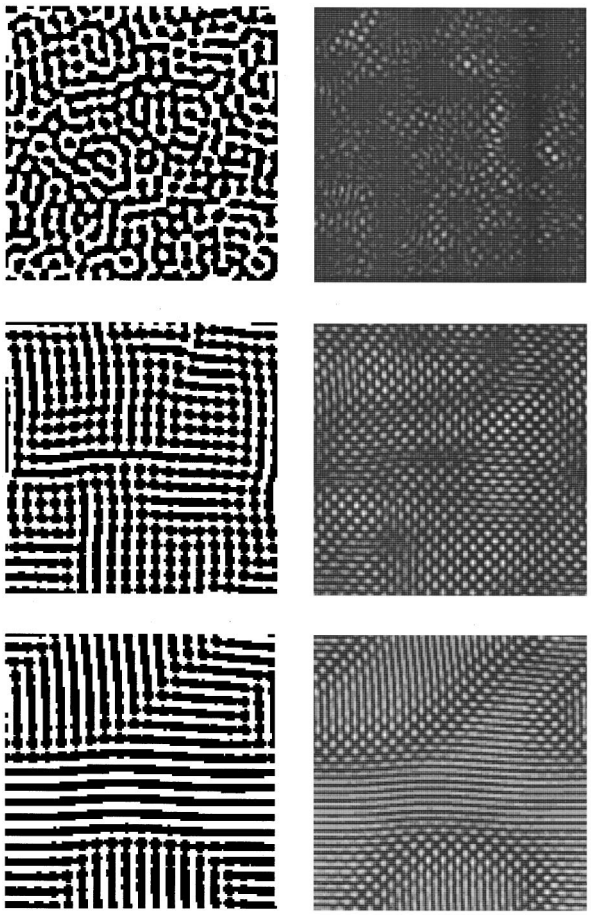

FIG. 14. The left column shows the concentration field and the right column is Q_E for the system with cubic anisotropy, in the near-onset regime. $v=0.24$, $g_E=0.05$, and $g_\xi=0.1$. Times from top to bottom are 50, 500, and 2000.

the difference in the shear modulus between the two phases (f_E). This interaction is cubic in ϕ and is of the form $g_E\Sigma_{i,j}\int\int\int d\mathbf{r}d\mathbf{r}'d\mathbf{r}'\phi(\mathbf{r})G_{ij}(\mathbf{r},\mathbf{r}')\phi(\mathbf{r}')G_{ij}(\mathbf{r}',\mathbf{r}'')\phi(\mathbf{r}'')$. It does not contribute to the linear dispersion relation; its effects are purely nonlinear. This can be seen in Fig. 9, where upon entering the nonlinear regime the stripes pinch away, fold, and form droplets. Calculations have shown that the interaction between two hard spherical precipitates in a soft matrix is *repulsively long range* and is mediated by the elastic fields.[19] However,[18] other authors have argued that this

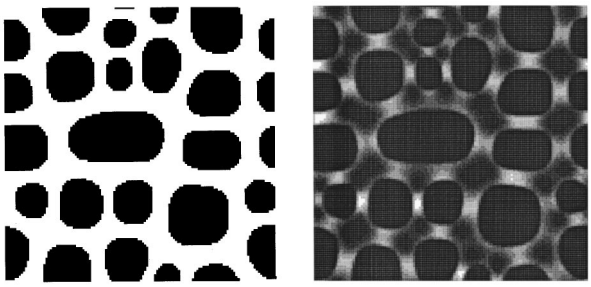

FIG. 15. The left panel shows the concentration field and the right panel is Q_E for the system with cubic anisotropy, in the far-from-onset regime. $v=0.001$, $g_E=0.05$, and $g_\xi=0.1$. The snapshots were taken at time=10 000.

interaction vanishes when the hard precipitates undergo shape changes from spheres to ellipsoids. As seen in our simulations, the hard precipitates do have a vanishing shear energy. This is not to say that the long-range elastic interaction vanishes in general, because deformations of the soft phase to accommodate the shape changes must also be taken into account. Although nothing can be said about f_E in terms of the full free-energy expression, we believe that f_E leads to long-range repulsive interactions between the precipitates.

For film growth, the presence of f_E is in competition with both the phase separation and the deposition process. As seen in our simulation results, this leads to a competition between steady-state lamellar phases and steady-state droplet phases. For deposition rates near the threshold for instability, the long-range elastic interaction creates the droplets; the long-range interaction due to the deposition then orders these droplets in an hexagonal array. Hence, the well-ordered hexagonal state is due to *both* long-range interactions. This means that if predictions for the selected wave number of the patterns are to be made, they should depend on the two parameters v and g_E.

V. CONCLUSION

To summarize, we have studied the growth by MBE of a thin solid layer composed of two different atomic types. The constant deposition of material competes with the phase segregation to produce modulated structures. Elastic effects due to a difference between the elastic moduli of the two components and crystal anisotropy were shown to modify the dynamical evolution and the steady state reached by the system. The elastic effects were directly responsible for the appearance of droplets of the hard phase in a soft matrix, while the crystal anisotropy favored spinodal decomposition along the soft directions, aligning the stripes or forming cuboidal droplets.

ACKNOWLEDGMENTS

This work was supported by the NSERC of Canada. F.L. also acknowledges support from the Walter C. Sumner fund.

APPENDIX A: DERIVATION OF THE EFFECTIVE FREE ENERGY FUNCTIONAL

In this appendix, we show how the displacement vector can be obtained in terms of the order parameter using the mechanical equilibrium condition, and derive the effective free-energy functional as a function of ψ only. We start with the expression for the stress tensor

$$\sigma_{ij}=\frac{\delta\mathcal{F}}{\delta\mu_{ij}}=[\alpha\psi+K\nabla\cdot\mathbf{u}+B\mu_{ii}]\delta_{ij}+2M\left(\mu_{ij}-\frac{\delta_{ij}}{d}\nabla\cdot\mathbf{u}\right). \tag{A1}$$

(Note that repeated indices do not imply summations and that in the anisotropy term $B\mu_{ii}$, the repeated index i is not summed). The mechanical equilibrium condition is

$$\sum_j \nabla_j\sigma_{ij}=\nabla_i[\alpha\psi+K\nabla\cdot\mathbf{u}]+B\nabla_i\mu_{ii}+2M\sum_j \nabla_j\left(\mu_{ij}-\frac{\delta_{ij}}{d}\nabla\cdot\mathbf{u}\right)=0, \tag{A2}$$

which can be written as

$$(K+M-2M/d)\nabla_i\nabla\cdot\mathbf{u}+B\nabla_i^2u_i+M\nabla^2u_i+\alpha\nabla_i\psi=0. \tag{A3}$$

The goal of our scheme is to calculate u_i in terms of ψ *to first order* in K_1, M_1, and B_1. To do so, we write $\mathbf{u}=\mathbf{u}^0+\mathbf{u}^1$, where $\mathbf{u}^1$ is of $O(K_1,M_1,B_1)$. To zeroth order in the coefficients M_1, K_1 and B_1, we have

$$(K_0+M_0-2M_0/d)\nabla\nabla\cdot\mathbf{u}^0+M_0\nabla^2\mathbf{u}^0+\alpha\nabla\psi=0, \tag{A4}$$

which can be solved for $\nabla\cdot\mathbf{u}^0$ by taking an extra divergence:

$$\nabla^2\nabla\cdot\mathbf{u}^0=-\frac{\alpha}{C_0}\nabla^2\psi, \tag{A5}$$

with the definition $C_0=K_0+2M_0(1-1/d)$. The general solution of this Poisson equation consists of a linear combination of the particular solution and the solution to the Laplace equation. Because of the periodic boundary conditions, the compression $\nabla\cdot\mathbf{u}^0$ and its first derivative are continuous at the boundaries, implying that the solution to the Laplace equation is zero everywhere. Hence, the solution for $\nabla\cdot\mathbf{u}^0$ is

$$\nabla\cdot\mathbf{u}^0=-\frac{\alpha}{C_0}\psi. \tag{A6}$$

Substitution of this expression for $\nabla\cdot\mathbf{u}^0$ in Eq. (A4) gives

$$u_i^0=-\frac{\alpha}{C_0}\nabla_i W, \tag{A7}$$

where W is obtained from

$$\nabla^2 W=\psi. \tag{A8}$$

To this lowest order, substitution into Eq. (1) leads to $\mathcal{F}_{\rm el}[\psi]=\int d\mathbf{x}f_0$ with

$$f_0=-\frac{\alpha^2}{2C_0}\psi^2 \tag{A9}$$

(integration by parts is necessary to obtain this result). We now proceed to calculate the corrections $\mathbf{u}^1$ due to the anisotropy and the difference in elastic moduli between the two phases. We separately calculate these corrections in order to make the derivations more transparent.

1. Corrections due to the anisotropy

To first order in B_1, $\mathbf{u}^1$ satisfies the equation

$$(K_0+M_0-2M_0/d)\nabla_i\nabla\cdot\mathbf{u}^1+B_1\nabla_i^2u_i^0+M_0\nabla^2u_i^1=0, \tag{A10}$$

with a solution

$$\nabla\cdot\mathbf{u}^1=\frac{\alpha\xi M_0}{C_0^2}\psi-\frac{\alpha\xi M_0}{C_0^2}\frac{1}{\nabla^2}\sum_{i\neq j}\nabla_i^2\nabla_j^2\frac{1}{\nabla^2}\psi. \tag{A11}$$

In this last equation, the operator $1/\nabla^2$ represents the inverse laplacian. Substitution of Eq. (A11) in Eq. (A10) leads to

$$u_i^1=\frac{\alpha\xi M_0}{C_0^2}\nabla_i\frac{1}{\nabla^2}\psi-\frac{\alpha\xi M_0}{C_0^2}\nabla_i\frac{1}{\nabla^4}\sum_{i\neq j}\nabla_i^2\nabla_j^2\frac{1}{\nabla^2}\psi, \tag{A12}$$

which is clearly first order in the anisotropy ξ. With the displacement vector determined as a function of ψ, we can substitute it back in the elastic free-energy functional and obtain an effective free-energy functional in terms of ψ only. We write the free-energy density as $f_{\rm el}=f_0+f_\xi$, with f_ξ of $O(\xi)$. To calculate f_ξ, notice that mechanical equilibrium requires $\delta\mathcal{F}/\delta u_i=0$, implying that

$$f_\xi=\frac{1}{2}B_1\sum_i\mu_{ii}^2=\frac{\alpha^2\xi M_0}{2C_0^2}\psi^2-\frac{\alpha^2\xi M_0}{2C_0^2}\sum_{i\neq j}(\nabla_i\nabla_j W)^2. \tag{A13}$$

2. Corrections due to the difference in the bulk moduli

In this case, $\mathbf{u}^1$ is of $O(K_1)$ and is a solution of

$$(K_0+M_0-2M_0/d)\nabla_i\nabla\cdot\mathbf{u}^1+M_0\nabla^2u_i^1+K_1\psi\nabla_i\nabla\cdot\mathbf{u}^0=0. \tag{A14}$$

Again, taking the divergence of this equation yields

$$\nabla\cdot\mathbf{u}^1=\frac{\alpha K_1}{C_0^2}\psi^2 \tag{A15}$$

and

$$u_i^1=\frac{\alpha K_1}{C_0^2}\nabla_i\frac{1}{\nabla^2}\psi^2. \tag{A16}$$

The correction to the elastic energy is

$$f_{K_1}=\frac{1}{2}K_1\psi(\nabla\cdot\mathbf{u}^0)^2=\frac{1}{2}\frac{\alpha^2K_1}{C_0^2}\psi^3. \tag{A17}$$

In the main text, we combine f_0 and f_{K_1}, and use the quadratic form $-\alpha\psi^2/2C$ with $C=K+2M_0(1-1/d)$.

3. Corrections due to the difference in the shear moduli

Here, $\mathbf{u}^1\sim O(M_1)$ satisfies

$$(K_0+M_0-2M_0/d)\nabla_i\nabla\cdot\mathbf{u}^1+M_0\nabla^2u_i^1+M_1\psi\nabla^2u_i^0+M_1\nabla_i\nabla\cdot\mathbf{u}^0=0, \tag{A18}$$

which gives

$$\nabla\cdot\mathbf{u}^1=\frac{2\alpha M_1}{C_0^2}\frac{1}{\nabla^2}\nabla_i\nabla_j\left[\psi\left(\nabla_i\nabla_jW-\frac{\delta_{ij}}{d}\psi\right)\right] \tag{A19}$$

and

$$u_i^1=\frac{2\alpha M_1}{C_0^2}\nabla_i\frac{1}{\nabla^4}\nabla_i\nabla_j\left[\psi\left(\nabla_i\nabla_jW-\frac{\delta_{ij}}{d}\psi\right)\right]. \tag{A20}$$

The contribution to the elastic energy of order M_1 is

$$f_{M_1}=M_1\psi\sum_{i,j}\left(\mu_{ij}^0-\frac{\delta_{ij}}{d}\nabla\cdot\mathbf{u}^0\right)^2=\frac{M_1\alpha^2}{C_0^2}\psi\sum_{i,j}\left(\nabla_i\nabla_jW-\frac{\delta_{ij}}{d}\psi\right)^2. \tag{A21}$$

[1] J. E. Guyer and P. W. Voorhees, Phys. Rev. Lett. **74**, 4031 (1995).

[2] T. Okada, G. C. Weatherly, and D. W. McComb, J. Appl. Phys. **81**, 2185 (1997).

[3] C. D. Adams, M. Atzmon, Y.-T. Cheng, and D. J. Srolovitz, J. Mater. Res. **7**, 653 (1992).

[4] F. Léonard, M. Laradji, and R. C. Desai, Phys. Rev. B **55**, 1887 (1997); F. Léonard and R. C. Desai, *ibid.* **55**, 9990 (1997).

[5] A. Onuki and H. Nishimori, Phys. Rev. B **43**, 13 649 (1991).

[6] I. P. Ipatova, V. G. Malyshkin, and V. A. Shchukin, J. Appl. Phys. **74**, 7198 (1993).

[7] A. Onuki, J. Phys. Soc. Jpn. **58**, 3065 (1989); **58**, 3069 (1989).

[8] C. Sagui, A. M. Somoza, and R. C. Desai, Phys. Rev. B **50**, 4865 (1994).

[9] L. D. Landau and E. M. Lifshitz, *Theory of Elasticity* (Addison-Wesley, Reading, MA, 1986).

[10] H. Nishimori and A. Onuki, Phys. Rev. B **42**, 980 (1990).

[11] Y. Oono and M. Bahiana, Phys. Rev. Lett. **61**, 1109 (1988).

[12] J. D. Gunton, M. San Miguel, and P. S. Sahni, in *Phase Transitions and Critical Phenomena*, edited by C. Domb and J. L. Lebowitz (Academic, London, 1983), Vol. 8, and references therein.

[13] A. Onuki, J. Phys. Soc. Jpn. **60**, 345 (1991).

[14] H. Nishimori and A. Onuki, J. Phys. Soc. Jpn. **60**, 1208 (1991).

[15] C. Yeung and R. C. Desai, Phys. Rev. E **49**, 2096 (1994).

[16] G. C. Hua, N. Otsuka, D. C. Grillo, J. Han, L. He, and R. L. Gunshor, J. Cryst. Growth **138**, 367 (1994).

[17] D. W. McComb, T. Okada, G. C. Weatherly, R. A. Wolkow, and J. E. Hulse, Philos. Mag. Lett. **73**, 129 (1996).

[18] A. Onuki and H. Nishimori, J. Phys. Soc. Jpn. **60**, 1 (1991).

[19] A. J. Ardell, R. B. Nicholson, and J. D. Eshelby, Acta. Metall. **14**, 1295 (1966).